



# Path dependence of the charge state distributions of low-energy $F^{q+}$ ions backscattered from RbI(100)

L.I. Vergara <sup>\*</sup>, F.W. Meyer, H.F. Krause

*Physics Division, Oak Ridge National Laboratory, Oak Ridge, TN 37831-6372, USA*

## Abstract

Projectile neutralization during backscattering from RbI(100) of F multicharged ions in the keV energy range was investigated utilizing a time-of-flight technique. The energy and charge state distributions of the scattered ions were measured as a function of the polar incidence angle and the target azimuthal orientation. We found significant variations in the neutralization degree for incident projectiles of different charge states. The charge state distribution of scattered ions, including negative charge states, was found to depend on both the polar incidence and azimuthal orientation angles. These variations are attributed to the particular hard and soft encounters with neighboring lattice sites at the target surface along the path of the ion. Sample data for few-keV  $F^{2+}$  and  $F^{7+}$  incident projectiles are presented to illustrate the underlying concepts.

© 2004 Elsevier B.V. All rights reserved.

*PACS:* 79.20.Rf; 34.50.Dy; 61.18.Bn

*Keywords:* Ion-surface scattering; Multicharged ions; Projectile neutralization; RbI; Fluorine

## 1. Introduction

In this article we present a brief overview of recent studies of projectile neutralization during large-angle backscattering interactions with an insulator surface, RbI(100), carried out at the ORNL Multicharged Ion Research Facility. In

contrast to measurements of projectile neutralization during grazing surface interactions [1], which involve a large number of lattice sites, our backscattering studies have as one of their goals, improved understanding of projectile neutralization in the limit of one or two surface-atom collisions. As shown in published results [2,3] for Au(110), such collisions can be identified by energy loss analysis of the scattered projectiles. It was further shown that information about projectile neutralization at several different distinguishable surface

<sup>\*</sup> Corresponding author. Tel.: +1 865 574 4781; fax: +1 865 574 1118.

*E-mail address:* [vergarali@ornl.gov](mailto:vergarali@ornl.gov) (L.I. Vergara).

lattice sites could be obtained from analysis of the target azimuth dependences observed for the various scattered charge states. Using classical trajectory Monte Carlo simulations, true binary and quasi-binary double collisions with the different surface lattice sites could be determined [2].

Extending our projectile neutralization measurements to alkali halide targets, we have tried to determine the effect of the reduced electron density characterizing such targets, and to assess the possibility of resolving the individual target constituents by energy loss analysis. Initial measurements [4] with CsI(100) could not resolve energy losses associated with scattering from the halogen and alkali sites due to the small mass difference of the target atoms. However, subsequent measurements [5] with a RbI(100) target showed clear resolution of halogen and alkali site scattering. This finding opened the door to a site-specific study of neutralization in quasi-binary double collisions, where the identity of the “hard” collision scattering site is determined by energy loss analysis, and the identity of the “soft” collision partner is selected by suitable azimuth orientation of the target relative to the projectile scattering plane. A  $\langle 100 \rangle$  direction selects an alkali–halogen or halogen–alkali collision sequence, and a  $\langle 110 \rangle$  direction selects a halogen–halogen or alkali–alkali sequence. Aspects of site-specific projectile neutralization are briefly discussed and illustrated below.

## 2. Experiment

The experiments were performed using the ORNL Multicharged Ion Research Facility (MIRF) [6]. The apparatus, described in detail elsewhere [7], implements an ultrahigh vacuum chamber ( $10^{-10}$  Torr) and a time-of-flight (TOF) analyzer with a floatable drift tube that allows simultaneous measurement of the energy and charge state distributions of projectiles [7] scattered from a RbI(100) single crystal surface. An important feature of this setup is the ability to analyze all scattered charge states, including neutrals, essential for complete determination of scattered charge fractions.

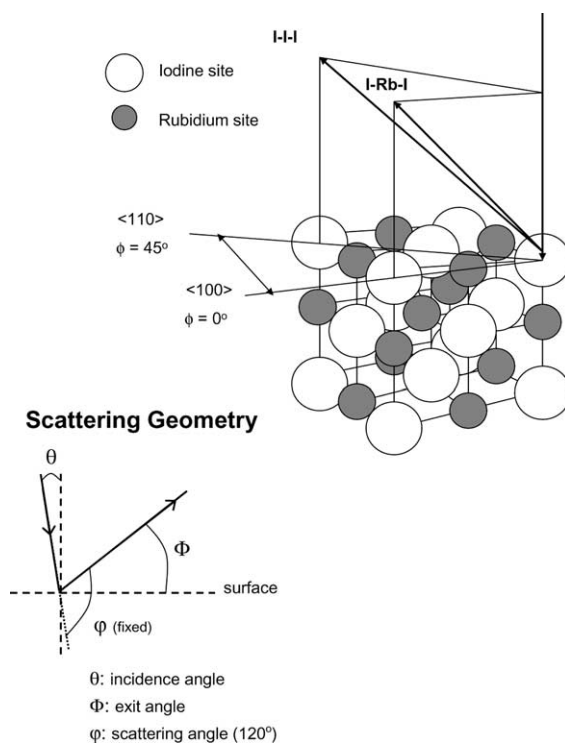


Fig. 1. Schematic diagram of the scattering geometry and the RbI(100) target showing the different atomic strings along a  $\langle 100 \rangle$  and  $\langle 110 \rangle$  direction.

The chopped primary ion beam is decelerated from  $(10 \times q)$  keV to final energies in the 4–5 keV range before impinging on the RbI(100) surface. The sample is mounted on a manipulator that allows variations of the ion incident direction with respect to the surface normal ( $\theta$ ) or to a main crystallographic axis ( $\phi$ ) (see Fig. 1). Ions and atoms scattered from the sample are detected by a multi-channel plate (MCP) located at a scattering angle of  $120^\circ$  from the incident beam direction.

In order to repair the induced-ion-bombardment damage from previous runs, before each measurement the surface was prepared using cycles of grazing bombardment with 2 keV  $\text{Ar}^+$  ions and annealing at  $450^\circ\text{C}$ . This method effectively removed impurities, and yielded very smooth ordered surfaces. To prevent macroscopic charging, the RbI target was maintained at a temperature of  $250^\circ\text{C}$  during the measurements.

### 3. Results and discussion

In Fig. 2 we show the TOF spectra for 4.2 keV  $F^{7+}$  and  $F^{2+}$  normally incident on the RbI(100) surface along the  $\langle 110 \rangle$  direction ( $\phi = 45^\circ$ ). These spectra are fairly typical for multicharged ion projectiles when a floatable drift tube is used. In the upper panel, the tube is biased at  $-3.0$  kV to resolve the different final positive projectile charge states from each other and from scattered projectiles backscattered as neutrals. In the lower panel, the tube is biased at  $+3.0$  kV. In this case, positively charged scattered projectiles do not reach the detector, while negatively charged projectiles are dispersed from backscattered neutrals. Since

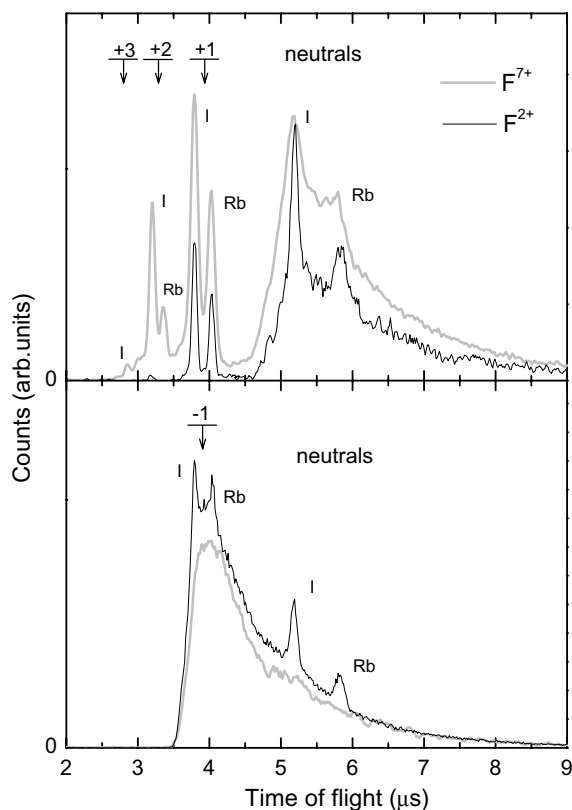


Fig. 2. Raw TOF spectra for 4.2 keV  $F^{7+}$  and  $F^{2+}$  normally incident on the RbI(100) surface, along the  $\langle 110 \rangle$  direction. Upper panel: drift tube biased at  $-3.0$  kV. Lower panel: drift tube biased at  $+3.0$  kV. The two panels have different (arbitrary) intensity scales.

the two surface constituents have significantly different masses, we can resolve F projectiles backscattered in a hard collision from either Rb or I atoms (site-specificity for each final charge state). Quasi-binary collision peaks associated with backscattering from Rb and I sites are clearly resolved for final charge states as high as  $3+$ . The scattered neutral binary collision peaks sit on top of a broad background structure which arises from multiple collisions whose trajectories extend deeper into the RbI bulk. The multiple collision background is not a significant feature for positive charged recoil ions, indicating that positive charged recoil ions do not survive in multiple collision cascades. However, the multiple collision background under the scattered negative binary collision peaks is very significant, and extends to larger flight times, obscuring the presence of the small neutral binary peaks which are evident for  $F^{7+}$  incident ions in the upper panel.

In order to obtain quantitative results for backscattered charge fractions, the TOF spectra are converted to energy spectra. As part of this transformation, the various scattered charge states are corrected for collection and detection efficiency effects [7]. The corrections can be significant and must be properly accounted to obtain an accurate

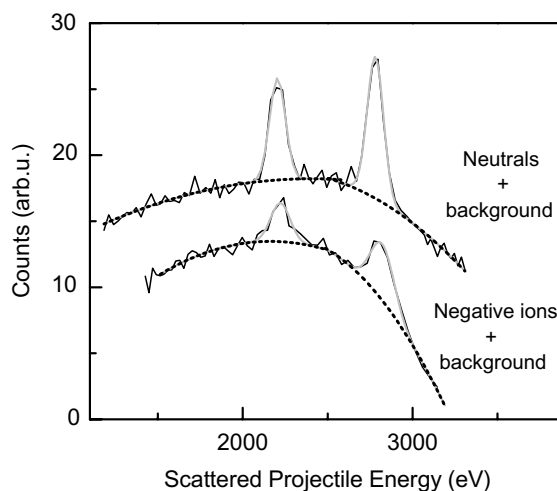


Fig. 3. Examples of fitting to energy spectra in order to determine the background, and consequently perform the background subtraction.

determination of scattered charge fractions. In addition, we perform a background subtraction to the energy spectra using a non-linear peak fitting algorithm consisting of a combination of polynomials and Gaussians. Examples of the fittings are shown in Fig. 3. Note the similarity between the backgrounds under the negative ions peaks and under the neutrals peaks: both originate from neutrals having undergone multiple collisions cascades.

Fig. 4 shows the background-subtracted recoil energy spectra derived from the TOF spectra of Fig. 2. In the two upper panels we show the neutrals and positively charged ions, and in the lower panels we show the neutrals and negatively charged ions. Analyzing these spectra we see that, in contrast to  $F^{2+}$ , for normally incident  $F^{7+}$  the formation of  $F^-$  ions in quasi-binary collisions is not detectable: no narrow peaks are discernible above the multiple collision background.

Moreover, the long-tailed background due to negative ions formed upon exiting the surface from neutrals having undergone multiple collisions cascades obscures the small quasi-binary collision neutral peaks. The absence of negative ions would not be surprising if the dominant charge state were  $3+$ , with sequentially decreasing amounts of  $2+$ ,  $1+$  and neutrals. But here just the opposite is the case: the lowest amount of detected ions corresponds to  $3+$  while neutrals are dominant. Thus, following the slope we would expect to detect  $F^-$ . On the other hand, the collision time for  $4.2$  keV fluorine ions and the Auger relaxation time, assuming an atom with a full M-shell and holes in the L-shell [8], are both  $\sim 2$  fs. This could explain the difference between the  $F^0$  states generated from  $F^{7+}$  and  $F^{2+}$ , since  $F^{2+}$  ions have no initial L-shell vacancies and thus are more likely to lead to already relaxed neutrals while  $F^0$  generated from normally incident  $F^{7+}$  is less likely to be fully

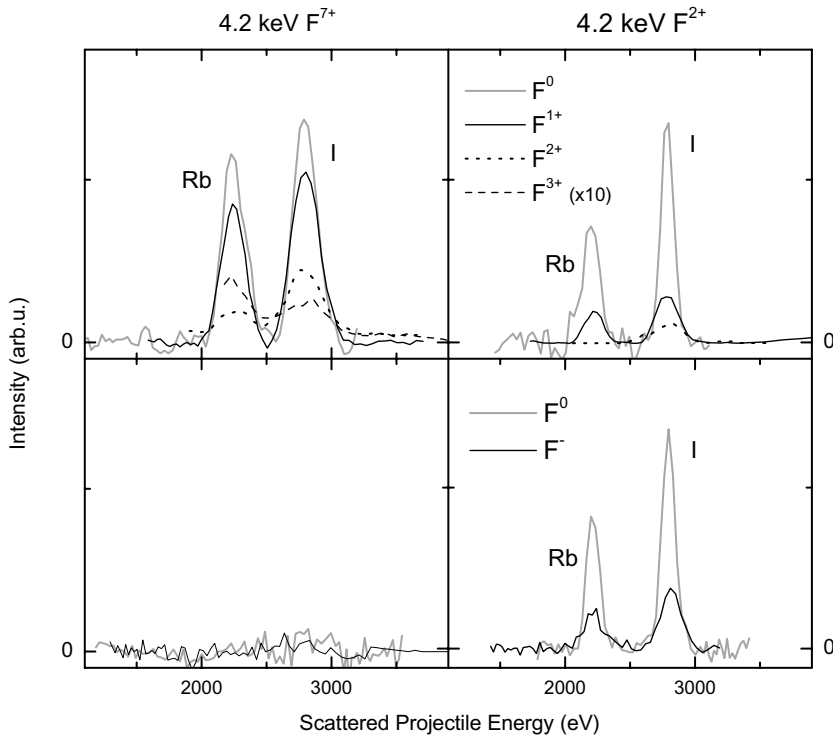


Fig. 4. Energy spectra of scattered neutral, and positive and negative charged ions obtained from the TOF spectra shown in Fig. 2 (normal incidence along the  $\langle 110 \rangle$  direction). Upper panel: obtained from TOF spectrum with drift tube biased at  $-3.0$  kV. Lower panel: obtained from TOF spectrum with drift tube biased at  $+3.0$  kV.

relaxed and to present a ground state core to which an additional electron can be captured on the receding trajectory.

We concentrate now our study on the  $F^{2+}$  projectile. One of the most noticeable results is the difference observed for the scattered charge states when changing the target azimuthal orientation, especially in the negative ion formation. In Fig. 5, energy spectra corresponding to normally incident 4.2 keV  $F^{2+}$  for two different azimuthal angles:  $\phi = 0^\circ$  ( $\langle 100 \rangle$  direction) and  $\phi = 45^\circ$  ( $\langle 110 \rangle$  direction), are shown. As we did previously, in the two upper panels we show the neutrals and positively charged ions and in the lower panels, neutrals and negatively charged ions. Along the  $\langle 100 \rangle$  direction, there seems to be no formation of  $F^-$  ions and no narrow peaks are discernible above the multiple collision background. On contrast, for scattering along the  $\langle 110 \rangle$  direction, we can observe both quasi-binary collision peaks:

the one corresponding to a hard collision with Rb, and the one corresponding to a hard collision with I. The differences in the charge transfer could be attributed to two things, a change in the passing distance from the next neighbor or the different type of collision that the projectile undergoes in each case. The azimuthal change from a  $\langle 100 \rangle$  to a  $\langle 110 \rangle$  direction changes the identity of the nearest neighbor atom, so that the sequence of quasi-binary collision changes from I–Rb or Rb–I to Rb–Rb or I–I. In the case of collisions of the type I–Rb or Rb–I (i.e. scattering along the  $\langle 100 \rangle$  direction), the passing distance to the second partner is 1.87 Å. In the case of collisions of the type I–I or Rb–Rb (i.e.  $\langle 110 \rangle$  direction), the passing distance to the second glancing scattering site is 2.6 Å (see Fig. 6(a)). Remarkably, even with a shorter passing distance, along the  $\langle 100 \rangle$  direction there is significantly less formation of  $F^-$  (actually none detectable above background), for both

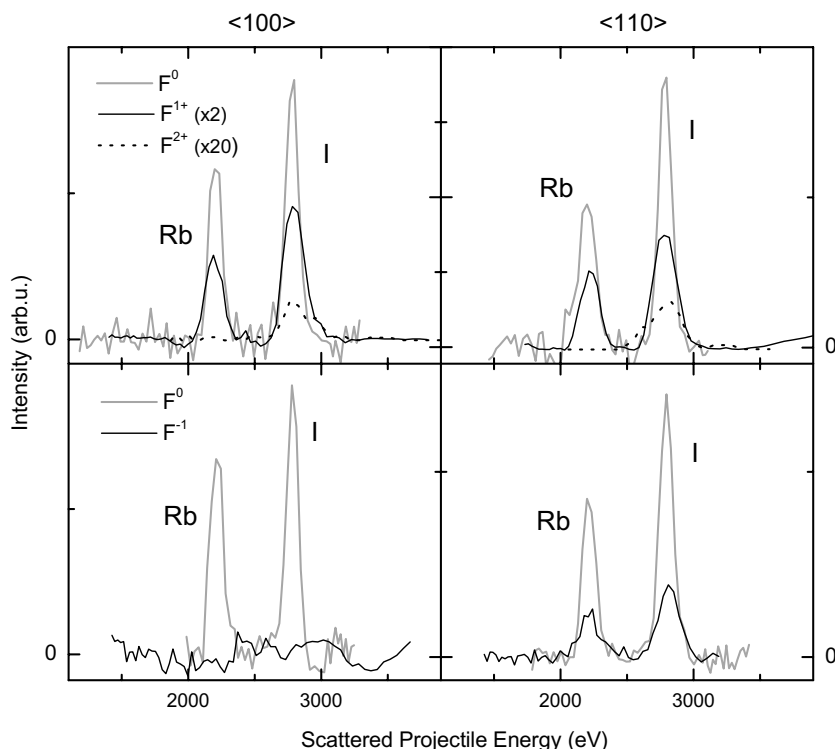


Fig. 5. Energy spectra for normally incident 4.2 keV  $F^{2+}$  scattered along two different azimuthal directions:  $\langle 100 \rangle$  and  $\langle 110 \rangle$ . Upper panels: neutrals and positive charge states. Lower panels: neutrals and negative charge states.

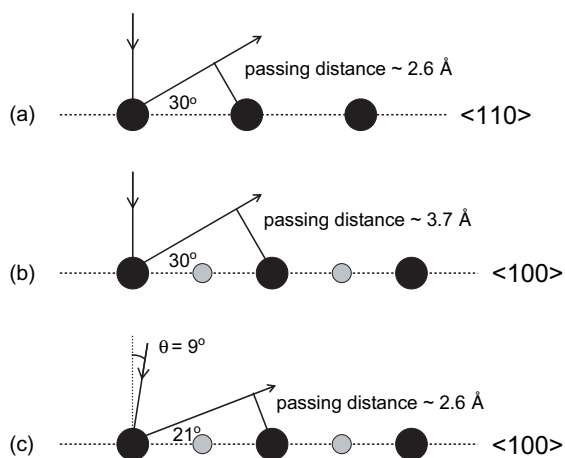


Fig. 6. Scheme of different RbI(100) surface scattering conditions: (a) normal incidence along the  $\langle 110 \rangle$  direction; (b) normal incidence along the  $\langle 100 \rangle$  direction; (c)  $9^\circ$  away from normal incidence along the  $\langle 100 \rangle$  direction.

collision sequences (i.e. I–Rb and Rb–I) than is observed for scattering along the  $\langle 110 \rangle$  direction. In order to simulate along the  $\langle 100 \rangle$  direction the same passing distance with same-species lattice sites (Fig. 6(b)) as obtained along the  $\langle 110 \rangle$  direction (Fig. 6(a)), measurements were made for an incidence angle of  $\theta = 9^\circ$  (Fig. 6(c)).

In Table 1 we show the charge fractions determined for each case. The fractions tabulated correspond to the sum of the projectiles scattered from Rb and I sites. As is evident from the table, when we go to more grazing exit trajectories along the  $\langle 100 \rangle$  direction, a significant increase in  $F^-$  production is observed, i.e. from 0%  $F^-$  charge fraction at  $30^\circ$  exit angle, to an  $F^-$  fraction of 43%

Table 1

Scattered charge fractions for incident 4.2 keV  $F^{2+}$ , under different surface orientations

Scattered charge state	$\langle 100 \rangle$	$\langle 110 \rangle$	$\langle 100 \rangle$
	$\theta = 0^\circ$	$\theta = 0^\circ$	$\theta = 9^\circ$
–1	0%	15%	43%
Neutrals	73%	61%	48%
+1	26%	23%	8%
+2	1%	1%	1%

The fractions tabulated correspond to the sum of the scattered fractions from Rb and I sites.

at a  $21^\circ$  exit angle. Moreover, the  $F^-$  charge fraction for the latter condition is  $\sim 3$  times bigger than that observed along the  $\langle 110 \rangle$  direction for a similar same-species passing distance (Fig. 6(a)). At present, it cannot be excluded that the increased  $F^-$  production is due to sub-surface layer contributions. Also, along the  $\langle 100 \rangle$  direction, electron capture from out-of-plane same-species sites, passed at a distance of 3.9 Å on the exit trajectory, may enhance the final  $F^-$  production.

Another remarkable feature of the present results is the similarity in the charge fractions obtained from quasi-binary collisions of the type I–I or Rb–Rb. This is surprising, since, unlike the I sites, the Rb sites have no loosely bound electrons to transfer. A possible explanation may again lie in the contribution of out-of-plane charge transfer events, since for a Rb–Rb in-plane collision sequence, one always has two out-of-plane iodine sites that are passed at almost the same distance as that of the second Rb site: 3.0 versus 2.6 Å. These two iodine sites may make significant contribution to the projectile neutralization.

The basis for the interesting trends described above will be explored in greater detail in upcoming experiments and simulations. A starting point will be the measurement of backscattered charge states for  $F^+$  as incident projectile. Since for a singly charged incident ion the interaction range can be expected to be smaller than for a multi-charged ion, the possible contribution from out-of-plane sites to projectile neutralization may be reduced, and thus lead to more pronounced site-specific neutralization differences. Also, Marlowe trajectory simulations [9] will facilitate the interpretation of the results and may uncover additional evidence of possible sub-surface layer contributions when we go away from normal incidence. In parallel with the experiments, extensions of the theoretical approach developed earlier for LiF surfaces [8] are planned to study the neutralization dynamics occurring during backscattering of ions from RbI.

## Acknowledgements

We are grateful to Dr. C.O. Reinhold for his suggestions and useful discussions. This research

was sponsored in part by the Office of Fusion Energy Sciences and by the Office of Basic Energy Sciences of the US Department of Energy under contract no. DE-AC05-00OR22725 with UT-Battelle, LLC. L.I.V. is appointed through the Oak Ridge National Laboratory Postdoctoral Research Associates Program administered jointly by the Oak Ridge Institute of Science and Education and Oak Ridge National Laboratory.

## References

- [1] L. Folkerts, S. Schippers, D.M. Zehner, F.W. Meyer, Phys. Rev. Lett. 74 (1995) 2204; Phys. Rev. Lett. 75 (1995) 983.
- [2] F.W. Meyer, V.A. Morozov, Nucl. Instr. and Meth. B 157 (1999) 297.
- [3] V.A. Morozov, F.W. Meyer, Phys. Rev. Lett. 86 (2001) 736; F.W. Meyer, V.A. Morozov, Nucl. Instr. and Meth. B 193 (2002) 530.
- [4] F.W. Meyer, V.A. Morozov, J. Mrogenda, C.R. Vane, S. Datz, Nucl. Instr. and Meth. B 193 (2002) 508.
- [5] F.W. Meyer, H.F. Krause, C.R. Vane, Nucl. Instr. and Meth. B 203 (2003) 231; Nucl. Instr. and Meth. B 205 (2003) 700; F.W. Meyer, H.F. Krause, V.A. Morozov, C.R. Vane, L.I. Vergara, Phys. Scr. T 110 (2004) 403; L.I. Vergara, F.W. Meyer, H.F. Krause, Surface and Coating Technology, in press.
- [6] F.W. Meyer, ECR-based atomic collision physics research at ORNL MIRF, in: J. Gillaspay (Ed.), Trapping of Highly Charged Ions Fundamentals and Applications, Nova Science Pub., New York, 2000, p. 117.
- [7] V.A. Morozov, F.W. Meyer, Rev. Sci. Instr. 70 (1999) 4515.
- [8] J. Burgdörfer, C.O. Reinhold, F.W. Meyer, Nucl. Instr. and Meth. B 205 (2003) 690.
- [9] M.T. Robinson, Radiat. Eff. Defect Solid 130 (1994) 3; Phys. Rev. B 40 (1989) 10717.